mpibp
max-planck-institut
für biophysik

GOETHE
UNIVERSITÄT
FRANKFURT AM MAIN

Bachelor Thesis

A Solid Supported Membrane based Electrophysiological Study of the *Escherichia coli* NhaA variant E241C

Marco Daniel Kokic

Department of Biophysical Chemistry
Max-Planck-Institute of Biophysics

I hereby declare that this thesis entitled "A Solid Supported Membrane based Electrophysiological Study of the *Escherichia coli* NhaA variant E241C" is the result of my own research except as cited in the references. This thesis has not been accepted for any degree and is not concurrently submitted in candidature of any other degree.

Student : Marco Daniel Kokic

Signature :

Date :

Supervisor : Prof. Dr. Klaus Fendler

Co-Supervisor : Prof. Dr. Werner Mäntele

For my mother, my sister and Jana

Abstract

The dependence of the *Escherichia coli* Na^+H^+ antiporter A (EcNhaA) pH sensor mutant E241C on H^+ and Na^+ concentrations was tested using a solid supported membrane (SSM) based electrophysiological approach. Proteoliposome preparations with right side out (RSO) oriented carriers were used to investigate the passive downhill uptake mode (physiologically the reverse transport mode) at zero membrane potential. Na^+ concentration gradients established with a rapid solution exchange acted as the driving force. When a Na^+ concentration gradient was established at symmetrical pH, the transport activity of the E241C EcNhaA variant was similar to that of the wildtype EcNhaA, with no shift of the bell-shaped pH dependence, an increase of the K_m^{Na} at acidic pH and a decrease of the K_m^{Na} at alkaline pH, supporting the model of a competitive binding of Na^+ and H^+ to a common binding site.

Contents

Abbreviations and Quantities

Å	Ångström (10^{-10} m)
APS	Ammonium persulfate
C	Cysteine (Cys)
D	Aspartate (Asp)
DEPC	Diethylpyrocarbonate
D-iLDH	NAD-independent D-lactate-dehydrogenase
DTT	Dithiothreitol
EcNhaA	*Escherichia coli* Na^+H^+ antiporter A
EDTA	Ethylenediaminetetraacetic acid
E241C	Glutamic acid 241 replaced by cysteine
g	G-force
H^+	Hydrogen ion
HCl	HCl (aq), Hydrochloric acid
HEPES	4-(2-hydroxyethyl)-1-piperazineethanesulfonic acid
H	Histidine (His)
I_{max}	Peak current at saturating Na^+ concentration
IPTG	Isopropyl β-D-1-thiogalactopyranoside
ISO	Inside out orientation (of the membrane protein), physiologically opposite direction
KCl	Potassium chloride
kDa	Kilodalton
K_D^{Na}	Dissociation constant of Na^+
K_m^{Na}	Na^+ concentration at which the transport rate is half maximum
KP_i	Potassium phosphate
LBK	Lysogeny broth (medium) with KCl instead of NaCl
LDS	Lithium dodecyl sulfate
LPR	Lipid-to-protein ratio
Lys	Lysine
MES	2-(N-morpholino)ethanesulfonic acid
mM	Millimolar

Abbreviations and Quantities

MOPS	3-(N-morpholino)propanesulfonic acid
Na^+	Sodium ion
NaCl	Sodium chloride
nA	Nanoampere
nF	Nanofarad
nS	Nanosiemens
nm	Nanometer
OD_{600}	Optical density at 600 nm
pA	Picoampere
PDB	Protein Data Bank
pH	Negative $\log_{10}$ of the concentration of H^+
pK_a	Negative $\log_{10}$ of the acid dissociation constant of an electrolyte
rpm	Revolutions per minute
RSO	Right side out orientation (of the membrane protein), physiological direction
SDS-PAGE	Sodium dodecyl sulfate polyacrylamide gel electrophoresis
Ser	Serine
SSM	Solid supported membrane
Thr	Threonine
TMS	Transmembrane segment
Tris	Tris(hydroxymethyl)aminomethane
TCDB	Transporter Classification Database
TEMED	N,N,N′,N′-Tetramethylethane-1,2-diamine
Tyr	Tyrosine
v_{max}	Maximum transport rate
(v/v)	Volume per volume
(w/v)	Weight per volume
wt	Wildtype

1 Introduction

1.1 Biological Membranes

The basic component of biological membranes are lipids, they constitute fundamental membrane properties such as topology and fluidity. Furthermore, membranes are loaded with a variety of integral and peripheral proteins and other molecules in differing number concentrations and polymerizates, which for their part influence membrane properties. Lipids are amphiphilic molecules, they exhibit spontaneous polymorphisms in aqueous solutions. Aggregation of lipids and membrane proteins to fluid mosaic membranes (Singer et al., 1972) reduces the contact area of their apolar parts with water. This effect is caused by the entropic force of the ambient system of water molecules. The most abundant bilayer membrane lipids are phospholipids, whose chemical structure can either be derived from acylglycerols, a sphingoid base or plasmalogens. The nonpolar intermediate part of a phospholipid bilayer poses a high resistance to charged particles (Goldup et al., 1970). This may be represented by an equivalent circuit, namely a capacitor with the conducting solutions and the isolating membrane (Fendler et al., 1993). Conductance and capacity of the membrane can be measured via electrodes.

1.2 Active Transport of Charged Solutes

Living cells depend on the limitation of passive diffusion in favor of a regulated transport across the membrane barrier. The majority of all membrane transport is controlled by carrier proteins and channel proteins which traverse the membrane lipid bilayer and thus facilitate the diffusion of selected solutes or actively transport them in an energy-driven process. The movement of ions in a fluid (i.e. relative to it) is induced by the electrochemical potential gradient which is established by concentration gradients of charged solutes. Generally, electrodiffusion is coupled to a one-way entropy gradient (for an adiabatic, irreversible process in an isolated system). Uphill transport against an electrochemical potential gradient involves a source of energy, which is ATP, light or redox energy in the case of primary active transporters and the coupled transport of two solute species in the case of secondary active transporters. In secondary active transport the downhill diffusion of one solute provides free enthalpy for the uphill transport of the other solute. This can occur either in the same direction or in the opposite direction and is referred to as symport and antiport. Many active transporters in bacteria that are driven by ion gradients are coupled to pH gradients, such as the symporter lactose permease (Booth et al., 1979) and the NhaA Na^+:H^+ Antiporter (NhaA) Family (TCDB family 2.A.33).

1.3 Na^+H^+ Antiporters

Na^+H^+ Antiporters are widely spread in the biological kingdoms. In Eukarya they are located either in cell or organelle membranes. They possess 10-12 transmembrane segments (TMS) and are classified as members of the cation proton antiporter families CPA1 (electroneutral) and CPA2 (electrogenic). It is thought that they catalyze substrate transport by conformational changes that give alternating access to a binding center from both sides of the membrane (Krishnamurthy et al., 2009). An important insight is that substrate binding lowers the activation energies between the conformers along the catalytic trajectory (Henzler-Wild and Kern, 2007; Zhao et al., 2011). Procaryotic cells such as *Escherichia coli* use both chemical and electrical potential gradients (membrane potential) for antiport processes to maintain homeostasis. In the proteome of *Escherichia coli* two Na^+H^+ antiporters were discovered, declarated EcNhaA (Taglicht et al., 1993) and EcNhaB (Pinner et al., 1994). Both are responsible for pH, cation and volume homeostasis and enable *Escherichia coli* to survive in environments such as the gastrointestinal tract of humans and many other warm-blooded animals.

Table 1: Characterization of *Escherichia coli* Na^+H^+antiporters (Classification according to the Transporter Classification Database TCDB).

Protein	Transporter Classification Superfamily	Antiport Process	Electrogenicity
EcNhaA	cation proton antiporter (CPA)	$Na^+/Li^+ \rightleftharpoons 2\,H^+$	1 e
EcNhaB	ion transporter (IT)	$2\,Na^+/2\,Li^+ \rightleftharpoons 3\,H^+$	1 e

1.4 The Na^+H^+ Antiporter A of *E. coli* (EcNhaA)

Especially in environments with higher salinity or alkalinity, EcNhaA is of vital importance (Padan et al., 2004). EcNhaA is an electrogenic transporter also capable of utilizing the energy of the membrane potential which is present in vivo (Taglicht et al., 1993) for its coupled antiport, i.e. an uptake of two H^+ and an extrusion of a Na^+. Due to its many homologues especially among Bacteria but also in Archaea such as *Haloarcula* which are extremely halophilic, or Eukaryota such as in most human tissue cells, and the degree of available structural information, EcNhaA serves as a prototype for several antiporters within the CPA superfamily (Brett et al., 2005). The expression of EcNhaA from the *nhaA* gene is triggered by a Na^+ specific regulatory system (Dover et al., 2001). EcNhaA also possesses a comparatively high turnover rate of up to 1000 s^{-1} (Taglicht et al., 1991).

1.4.1 Structure

The structure of EcNhaA has been resolved via X-ray diffraction (Hunte et al., 2005) and electron crystallography (Appel et al., 2009). It consists of 388 amino acids with a molecular weight of 41.4 kDa building a 40x45x50 $Å^3$ multipass protein. Between the N- and C-terminal cytoplasmic coils, 12 tilted alpha-helices (TMS I-XII) are grouped into two topologically inverted repeats and are interspersed with cytoplasmic and periplasmic loops and two discontinuous helices (TMS IV/XI assembly). D163 and D164 on TMS V are an important part of the supposed substrate binding site (Hunte et al., 2005). On the periplasmic membrane surface, between TMS I and II, a topological domain of two antiparallel beta-sheets is responsible for the dimerization of EcNhaA monomers, together with a group of amino acids on the cytoplasmic side of TMS VII and IX (Hilger et al., 2005 and 2007). A comparison of the helix packing of detergent solubilized 3D crystals (from X-ray diffraction) at pH 4 and lipid solubilized 2D crystals (from electron crystallography, crystals grown at pH 4 and incubated at higher pH) indicates that EcNhaA is in a native conformation in the 3D crystals (Screpanti et al., 2006). The less than average resolution (PDB status as of April 2013: 78965 released structures, Mean 2.19 Å, Std. Dev. 1.15 Å) of the EcNhaA 3D crystal X-ray diffraction data of 3.45 Å is indicative of EcNhaA instability in the detergent which may partly be linked to EcNhaA dynamics (Kang et al., 2013).

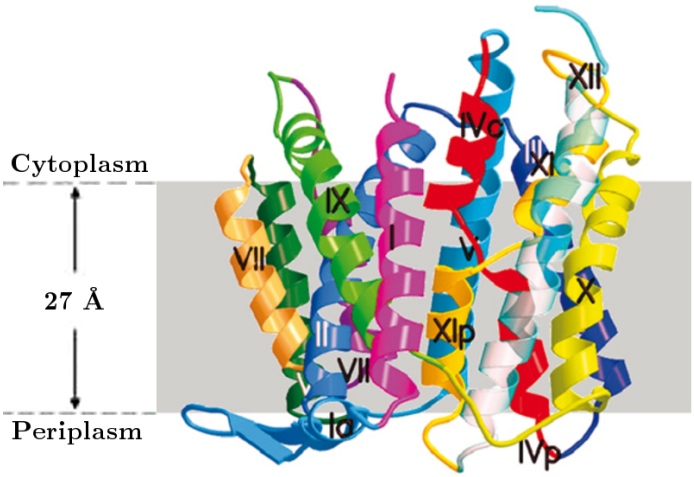

Figure 1: 3D Crystal Structure of EcNhaA (PDB entry 1zcd) at pH 4, stereo view of a ribbon representation viewed parallel to the membrane. TMS IV/XI assembly (red and yellow-orange) is located in the center of EcNhaA. Its short coils and Asp 163 and Asp 164 from TMS V constitute the substrate binding region. Image taken from Hunte et al., 2005.

1.4.2 Functional Properties

EcNhaA shows a distinct dependence on H^+ concentration as has more recently been experimentally verified by detailed SSM electrophysiological studies of the wildtype (Ganea et al., 2009; Mager et al., 2011). In the presence of 10 and 100 mM Na^+ concentrations wildtype EcNhaA has its optimum at pH 8.7. Between pH 8.5 and pH 7 the activity decreases by more than 80% and an inactivation occurs at symmetric H^+ concentrations below pH 6.5. Above pH 9 the activity decreases again, displaying a symmetric bell-shaped pH profile. These results are in accordance with previous findings (Taglicht et al., 1993). The SSM electrophysiological studies also showed that the v_{max} did not change significantly ($\pm 30\%$) below pH 9 but the K_m^{Na} rose more than 600% from pH 8.5 to pH 7.5. This means that the catalytic efficiency (k_{cat}) of EcNhaA stays high over a large part of its pH range and only decreases at alkaline pH above pH 9.

$$k_{cat} = \frac{v_{max}}{[\text{EcNhaA}]} \tag{1}$$

1.4.3 Suggested Transport Mechanisms

The Allosteric Regulation Model

The allosteric regulation model is based on the assumption of a pH sensor region located on the cytoplasmic side of EcNhaA that, caused by its protonation state, downregulates transport activity below pH 8.5 to complete inactivation at pH 6.5 by triggering a conformational change (Hunte et al., 2005; Padan et al., 2009).

The Competitive Binding Model

The competitive binding model of the EcNhaA transport mechanism was developed by Ganea and Fendler (2009) and experimentally and by means of a minimal kinetic model supported by Mager et al. (2011). First of all, a high similarity of the transport parameters for forward and reverse transport suggest a single substrate binding site for both transport directions. Secondly, the dependence of K_m^{Na} on H^+ concentration is large in comparison to the dependence of v_{max}. pH lowering goes together with a K_m^{Na} increase and at alkaline pH values the K_m^{Na} decreases. At asymmetric H^+ concentrations, EcNhaA is active at acidic pH even below pH 6.5. Enzyme activity is a function of the concentration of the (supposedly Na^+ bound, according to Hunte et al., 2005) active conformation of EcNhaA. The concentration of the active conformation can be calculated as a function of a coupled Na^+ and H^+ equilibrium binding, i.e. the competitive binding of Na^+ and H^+.

1.5 The EcNhaA E241C Variant

It has been shown that loop VIII-IX undergoes pH induced conformational changes (Gerchman et al., 1999). A replacement of glutamic acid at position 241 in loop VIII-IX with cysteine (E241C) caused a change of the pH dependence of EcNhaA in form of an acidic shift of 0.5 pH units in comparison to the wildtype, wich was taken as an indicative of a pH sensor functionality (Gerchman et al., 1999).

2 Motivation and Goal Settings

Due to their essential role for cell survival Na^+H^+ antiporters are important drug targets. Research results on EcNhaA transport and regulation mechanisms serve as reference for orthologues in many species. It has been shown that EcNhaA is highly pH dependent. From its inactivation at high H^+ concentrations an allosteric pH regulation model was deduced. It has been stated that loop VIII-IX (amino acids 237-245) plays a role as a so called pH sensor. In the course of this bachelor thesis the activity profile of the right side out oriented E241C EcNhaA pH sensor mutant was measured to find out whether the substitution amounts to changes of the transport parameters with respect to pH. Furthermore, the comparison of transport parameters of wildtype EcNhaA and E241C EcNhaA is used to support a minimal symmetrical kinetic model of regulation and transport, which is based on the assumption of a competitive binding of Na^+ and H^+ to a shared binding site.

3 Materials and Methods

3.1 Protein Preparation

3.1.1 Bacterial Culture and EcNhaA Expression

For the expression of the E241C NhaA variant a bacterial strain (*Escherichia coli* K-12 derivative: TA16) was cultivated according to the following procedure. A preparatory culture of the *E. coli* host was prepared with cells from a cryo stock which were inserted to 5 ml of LBK medium (100 µg/ml Carbenicillin) with an inoculating loop. Then the preparatory culture was shaken for six hours at 37 °C. 3 ml Carbenicillin (100 mg/ml) were added to 3 l of LBK medium (stock medium) and the preparatory culture was inserted into a flask with 0.5 l of stock medium and stirred over night at 180 rpm and 37 °C. The next day 30 ml of the 0.5 l preparatory culture were added to two flasks that each contained 1 l stock medium and stirred for two hours. At an OD_{600} between 0.3 - 0.9 during the exponential phase of bacterial growth 1M of IPTG (0.5 ml/l) was added to induce protein expression and the liquid culture was incubated for two hours. After reaching the stationary phase ($OD_{600} >$ 1.2), the liquid culture was centrifuged for 25 minutes at 5005 g (*Sorvall*). The moist mass of the remaining pellet was weighed and a fivefold amount of TSC buffer (10 mM Tris-HCl pH 7.5, 250 mM sucrose, 140 mM choline chloride) was added. The resulting suspension was flash frozen in liquid nitrogen and stored at -80 °C until further use.

3.1.2 Cell Disruption and Ultracentrifugation

After the EcNhaA expression the bacterial suspension was centrifuged at 2700 g for 25 minutes, the moist weight of the resulting pellets was determined and they were resuspended in a fivefold volume of TSCA buffer (10 mM Tris-HCl pH 7.5, 250 mM sucrose, 140 mM choline chloride, 125 µl DNAse, 1mM DTT, 2.5 mM $MgCl_2$ and protease inhibitor cocktail (*Complete Mini EDTA free, Roth*)). The suspension was then passed repeatedly through a narrow valve at a pressure of 1380 bar in a French Press (*SLM-AMINCO*) until it changed its color from yellow to brown. The whole procedure was conducted in a cooling room to avoid possible heat damage of the proteins. The homogenizate was then centrifuged for 10 minutes at 10.509 g and 4 °C to eliminate coarser cell debris, which then sedimented. The supernatant was then ultracentrifuged at 40.000 rpm in a 45 Ti rotor (*Beckman Coulter*) at 4 °C for one hour. The remaining pellet was then resuspended in TSC buffer (10 mM Tris-HCl pH 7.5, 250 mM sucrose, 140 mM choline chloride).

3.1.3 Bradford Protein Assay

The membrane protein concentration was quantitatively determined with the Bradford protein assay. Protein suspension was added to a solution containing phosphoric acid, ethanol and protonated Coomassie Brilliant Blue G-250 (*Bio-Rad Laboratories, Inc.*). The absorbance maximum of protonated Coomassie Brilliant Blue G-250 lies at 465 nm. It shifted from 465 nm to 595 nm when protein suspension was added to the solution due to a complex formation between proteins and the anionic form of Coomassie Brilliant Blue G-250. As the assay provides a linear estimate for protein concentrations over the tenfold concentration range of the reference protein bovine serum albumin, the sample was diluted and its concentration was set to 10 mg/ml.

3.1.4 Preparation of *E.coli*-Lipid Liposomes

A concentration of 20 mg/ml *E. coli* polar lipid extract in chloroform (*Avanti*) was swept by a stream of nitrogen gas under rotation (*Rotavapor R-114, Büchi*) until the chloroform volatilized. In the next step, reconstitution buffer (25 mM Hepes, 25 mM Tris-HCl, 100 mM KCl and 1 mM DTT, pH 7) was added to obtain a lipid concentration of 10 mg/ml. Then the lipid solution was shaken for 30 minutes at 4 °C (*VXR basic Vibrax, IKA*) and sonicated (*Ultrasonic cleaner, Laboratory Supplies*) until the lipid solution homogenized. Extrusion of the lipid solution (*Liposofast, Avestin*) with a polycarbonate membrane with a pore diameter of 400 nm finally produced unilamellar liposomes.

3.1.5 Measurement of Liposome Dimensions

The hydrodynamic radius of the prepared unilamellar liposomes was identified by means of dynamic light scattering (*ZetaPlus Zeta Potential Analyzer, Brookhaven Instruments*). 800 µl of the liposome suspension were pipetted into an acrylic cuvette and the measurement was conducted three times for 2 minutes. The extruded liposome suspension wich possessed a gaussian particle size distribution was then analyzed with the *ZetaPlus Particle Sizing Software*, which yielded a mean liposome diameter of about 200-300 nm.

3.1.6 Reconstitution of EcNhaA into Liposomes

His_6 tagged E241C EcNhaA were purified (from protein suspension prepared in 3.1.2) by Dr. Thomas Mager with the Ni^{2+} Nitrilotriacetic acid (Ni-NTA) affinity chromatography method. For the reconstitution of E241C EcNhaA into the preformed liposomes 1% (w/v) octyl D-glucopyranoside and E241C EcNhaA were added in a 10:1 lipid-to-protein mass ratio (LPR = 10). Detergents were removed by an addition of 30% (v/v) polystyrene beads (*SM-2*

adsorbent, Bio-Rad, Hercules) and the reconstitution preparation was shaken overnight at 4 °C. Then the polystyrene beads were replaced with new ones and the preparation was shaken for another hour. The polystyrene beads were removed and the preparation was centrifuged at 52.000 rpm and 4 °C for one hour (*TLA 100.2 rotor, Beckman Coulter*). The pellet was resuspended in NA buffer (300 mM KCl, 75 mM MOPS, 5 mM $MgCl_2$ and 1 mM DTT, pH 7) to a final lipid concentration of 5 mg/ml, shock-frozen in liquid nitrogen and stored at -80 °C. It has been shown by Zuber et al. (2005) that EcNhaA incorporates into liposomes in right side out (RSO) orientation.

3.1.7 Checking for EcNhaA with SDS-PAGE

In order to verify the presence of EcNhaA in the proteoliposomes (5mg/ml), 5 µl fourfold concentrated LDS loading buffer (*Invitrogen*) were added to 15 µl of proteoliposome suspension. 4-12% Bis-Tris agarose gel, MOPS-SDS (50 mM MOPS, 50 mM Tris, 1 mM Na-EDTA, 0.1% SDS) and *PageRuler Prestained Protein Ladder* standard (*Invitrogen*) were used. SDS-PAGE was carried out at 120 mA for 45 minutes and stained with Coomassie Brilliant Blue R-250 (*Bio-Rad Laboratories, Inc.*) over night. A decoloration was performed with 40% (v/v) ethanol and 10% acetic acid for 5-6 hours. Two distinct bands at $\approx$ 35 kDa and $\approx$ 55 kDa appeared which represent the monomer and dimer of EcNhaA. The discrepancy of the apparent molecular weight and the formula molecular weight (1.4.1) is known for membrane proteins ("gel shifting") and is caused by incomplete denaturation by SDS (Rath et al., 2009).

3.2 Measurement Buffer Preparation

During SSM measurements substrate concentration jumps were carried out by means of a rapid exchange between non-activating (NA) solutions without Na^+ substrate and activating (A) solutions with Na^+ substrate (see 3.2.2). An identical ionic strength of both NA and A solutions needed to be established to reduce solution exchange artifacts. The preparation of a common stock solution was a reasonable approach.

3.2.1 Stock Solutions

Stock solution for all buffers contained 25 mM Tris, 25 mM MOPS, 25 mM MES, 5mM $MgCl_2$ and 1 mM DTT. Magnesium chloride was added to reduce artifacts (forms complex with phosphatidylcholine) and DTT, a reducing agent, to avoid the oxidation of solvent-accessible thiol groups. The substances were dissolved in 90% of the desired solvent volume, filtrated (2 µm pore filters) and distributed in 8 aliquots according to the investigated pH range from pH 6 to pH 9.5 in 0.5 increments. After pH adjustment with HCl or Tris all

aliquots were filled up to the in sum desired total volume. All aliquots with their respective pH were then divided into quota for activating and non-activating buffer.

3.2.2 Activating and Non-Activating Buffers

Activating (A) and non-activating (NA) buffers were prepared by adding NaCl and KCl molarities to the stock solutions. NaCl concentrations in the activating buffers were replaced by identical concentrations of KCl in the non-activating buffers. The activating buffers contained x mM NaCl and $300 - x$ mM KCl. The non-activating buffers contained 300 mM KCl.

3.3 Solid Supported Membrane (SSM) Electrophysiology

3.3.1 Method Overview

The applied electrophysiological technique is based on a solid supported membrane (SSM) which serves as an adsorbent for EcNhaA proteoliposomes. The SSM setup allows a quick solution exchange between the non-activating solution and the substrate containing activating solution, which leads to an active substrate transport across the liposomal membrane. The substrate concentration rise time near the membrane during a solution exchange lies in the order of 10^{-2} to 10^{-3} seconds, which is actually the limiting factor for SSM electrophysiological measurements (Schulz et al., 2008). The net charge transfer across the liposomal membrane can be measured utilizing the capacitive coupling of the SSM/proteoliposome compound (Fendler et al., 1993). The solid supporting the adsorbent acts a measuring electrode, a grounded Ag/AgCl electrode as a reference (see Figs. 3, 4 and 5).

3.3.2 SSM Setup

The whole setup is shielded by a faraday cage. It consists of the fluid pathway (Fig. 2) and the SSM cuvette (Fig. 3). Outside the Faraday cage a current amplifier, valve controls, a function generator (to measure SSM conductance and capacitance) together with a computer (signal recording and valve control) were connected to the SSM setup (Fig. 2).

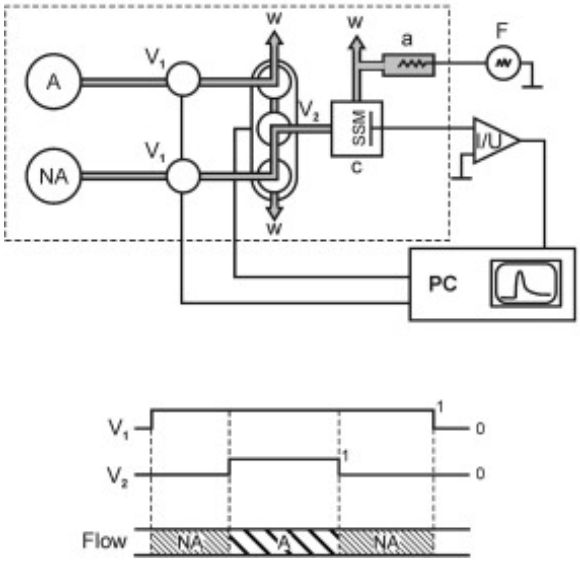

Figure 2: The fluid flow system of the SSM setup. Activating (A) and non-activating (NA) solutions are pumped through the SSM cuvette according to the rapid solution exchange protocol depicted beneath. (w) waste, (v_1) + (v_2) valves, (a) reference electrode, (F) function generator, (c) SSM cuvette, (PC) computer for signal recording and valve control. Image taken from Schulz et al., 2008.

SSM Cuvette The SSM cuvette is composed of an upper and lower panel, the sensor chip and the attached reference electrode part.

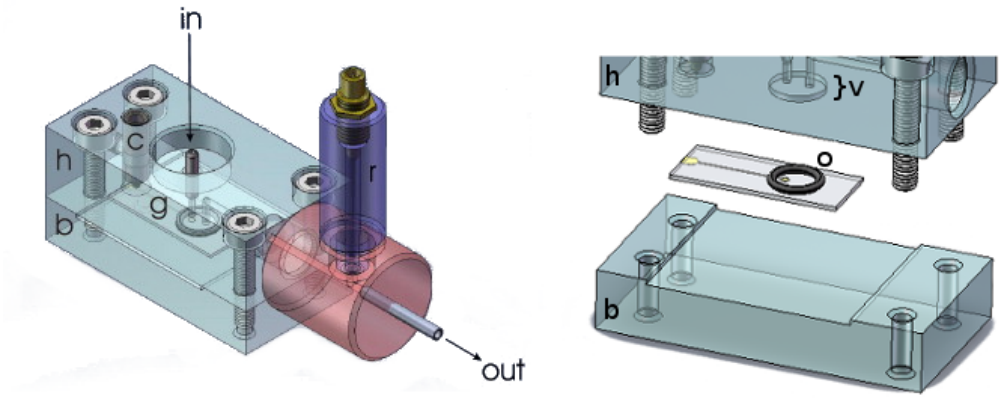

Figure 3: On the left: 3D model of the SSM cuvette. The Arrows denote the flow direction. (h) cuvette head, (b) cuvette base, (c) spring contact pin connection to the gold electrode on the sensor chip (g) , (r) gel bridge with reference electrode. On the right: Disassembled SSM cuvette with cuvette head, sensor chip and cuvette base. (v) cylindric volume for SSM measurements with inlet and outlet bores, (o) rubber ring. During measurements the SSM is located directly under the inlet bore. First image taken from Schulz et al., 2008; second image with kind permission of Prof. Fendler.

Improvements to the SSM Cuvette

In the course of the preparatory steps of the SSM cuvette a technical difficulty turned up occasionally. An untrained experimenter could crack the sensor chip whose substrate consists of borosilicate glass (Fig. 5). During fixation of the sensor chip between the top and bottom parts of the cuvette, the bolts are to be screwed in gradually at the same extent to prevent shear forces and consequently, rupture. A modification to the bottom part of the cuvette was proposed and realized to facilitate cuvette assembly. As the bottom part consists of polymethyl methacrylate (plexiglas), a cuboid with the dimensions of the sensor chip (+0.1 mm) was milled out. Consequently, shear forces on the cuvette when fixing it to the SSM setup and possible leakage were also prevented, as the cuvette parts could be screwed together more tightly.

Ag/AgCl Reference Electrode

A silver wire was worked with a fine sandpaper, then anodized in an HCl solution to coat it with AgCl. Afterwards the Ag/AgCl electrode was assembled and inserted into the gel bridge shown in Fig. 4. The gel bridge contained a selectively permeable barrier consisting of an acrylamide gel which was prepared as follows. The gel bridge was first cleaned with compressed air. Then 100 mM choline chloride and 100 mM KCl were added to a beaker containing 1.25 ml of 100 mM KP_i buffer (pH7) and 0.33 ml of 30% acrylamide/N,N'-methylenebisacrylamide were added. The solution was poured into the gel bridge. In the next step 0.05 ml of 10% APS (polymerization initiator, radical) and 10 µl TEMED (polymerization catalyst) were pipetted into the gel bridge to start the polymerization reaction. The solution then quickly solidified.

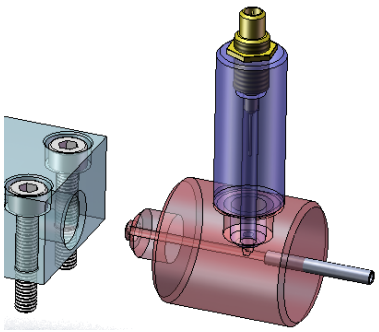

Figure 4: Reference electrode part of the SSM cuvette. The reference electrode and the acrylamide salt bridge sit inside the gel bridge which is connected perpendicularly to the main fluid pathway (directed from left to right). Image taken from Schulz et al., 2008.

3.3.3 Preparation of SSM Lipid Solution

For a lipid solution of 15 mg/ml and 1:60 (w/w) octadecylamine 375 µl of a diphytanoyl-phosphatidyl-choline stock solution (20mg/ml in chloroform) and 25 µl of octadecylamine (5 mg/ml in chloroform) were added to a vial. The chloroform was removed by a gentle stream of nitrogen gas and 500 µl of n-decane were added.

3.3.4 Preparation of the SSM

The sensor chip was incubated in a 1 mM octadecanethiol-ethanol solution for several hours. Afterwards it was rinsed carefully with ethanol and swept by a stream of nitrogen gas until it had dried. Then 1 µl of the SSM lipid solution was pipetted directly onto the gold tip of the chip. The octadecanethiolate molecules bind semi-covalently to Au atoms to form the solid supported membrane (self-assembled monolayer).

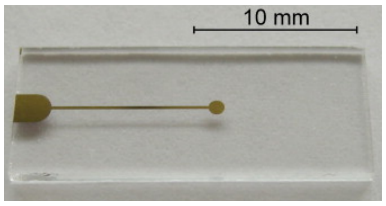

Figure 5: The sensor chip consists of a borosilicate glass substrate coated with a gold layer supported by an adhesive chromium layer. The electrode contact pad on the left is connected via a thin strip with the circular SSM on the right. Image taken from Schulz et al., 2008.

3.4 Electrophysiological Measurements

After inserting the sensor chip into the SSM cuvette and mounting the cuvette into the SSM setup, the flow system was activated and a couple of solution exchange cycles were executed to rinse the SSM. A function generator (*MPI of Biophysics*) was connected to the reference electrode to obtain the membrane parameters. A membrane capacitance between 300-500 nF/cm^2 when exposed to a triangular voltage of 50 mV and a membrane conductivity between 50-100 nS/cm^2 when exposed to a 100 mV square wave voltage qualified for the feasibility of the SSM measurements. In the following step 30-45 µl of RSO proteoliposome suspension (5 mg/ml, LPR = 10) were injected into the outlet bore of the SSM cuvette. 2-3 hours at room temperature were estimated for the adsorption of the proteoliposomes to the SSM.

3.4.1 Signal Recording Procedure

A quick solution exchange excited transporter activity. The net charge transfer across the liposomal membranes represented by the total current flow in the circuit was amplified by $10^8 - 10^{10}$ V/A and current frequencies above 2000 Hz were attenuated by a low pass filter. The pressure of the flow system was kept at 0.55 bar throughout the measurements. All measurement series were conducted under the same conditions with the exception that different sensor chips were used to avoid influences of material defects. The measurement values for each substrate concentration consisted of three averaged single measurement values.

3.4.2 Signal Correction

Solution Exchange Artifacts

The inrush of Na^+ during the solution exchange excited positive transient currents which are caused by interactions between the ions and the SSM. These Na^+ solution exchange artifacts showed a linear dependence on Na^+ concentration (Garcia-Celma et al., 2007). Furthermore, the artifact amplitude was smaller by one order of magnitude and did not significantly superimpose the recorded peak currents (see Fig. 8, left image). Therefore, in the course of measuring membrane parameters before the adsorption of the proteoliposomes, the Na^+ solution exchange artifact of a 100 mM Na^+ concentration jump was measured to correct the peak currents at a later point.

Amplitude Increase and Decrease

At times, the amplitude increased during a series of measurements. An explanation might be reordering processes of stacked proteoliposomes, e.g. at the beginning of a series of measurements several layers of proteoliposomes obstructed substrate dispersion and transport activity. After a series of solution exchanges overlying layers may have been washed away and the amount of active transporters and the total current signal were rising. Vice versa the amplitude could have decreased in the course of measurements due to washing away or inactivation of transporters at measurements for longer periods of time, like a couple of hours. Based on the measured linearity of decreases below 30%, the amplitudes of the initial measurements served as reference points and were divided by the amplitudes of later measurements at the same pH to obtain correction factors as a function of time. With these data points correction factors for all pH values could be acquired by means of a linear regression.

3.5 Kinetic Analysis

3.5.1 pH Dependence

Three peak currents were recorded at every pH during a pH dependence measurement series on a sensor chip and were averaged and normalized to the scaling parameter of the minimal symmetrical kinetic model fit (3.5.3 and Fig. 15) and to their maximum value at 100 mM Na^+. The scaling parameter quantifies varying overall transporter activity between the different sensors. Finally, the averaged and normalized values from three measurement series on different sensors were averaged.

3.5.2 Na^+ Dependence

A hyperbolic function was fitted to the averaged peak currents from each sensor to obtain K_m^{Na}:

$$y = I_{max} \cdot \frac{x}{K_m^{Na} + x} \tag{2}$$

Where x stands for the Na^+ concentration, y for the peak amplitude and I_{max} for the peak current at saturating Na^+ concentration. As the I_{max} varied among different measurement series, they were normalized to a constant saturation value of 1. Then, $\frac{y}{I_{max}}$ represents the normalization. The normalized values of three measurement series on different sensors were then averaged and the standard deviation σ was calculated. To identify changes of v_{max} the I_{max} values for 100 mM Na^+ concentration jumps at pH 7.5 and pH 9 were determined with the same sensor and the relative I_{max} value was calculated. The relative values from three measurement series on different sensors were then averaged.

3.5.3 Fitting to the Minimal Symmetrical Kinetic Model

The minimal symmetrical kinetic model used here for an analytical solution was developed by Mager et al. (2011) according to the model of a competitive binding of Na^+ and H^+ to a common single binding site as described in (1.4.3). Symmetrical means in this context that the transport parameters for forward and reverse transport direction are similar due to the symmetrical transport activity (i.e. bell-shaped pH dependencies) of wildtype EcNhaA using RSO and ISO proteoliposomes with zero membrane potential (see Mager et al., 2011). The analytical solution of the kinetic equations based on the minimal symmetrical kinetic model are the calculated substrate dependencies of the transport rate per mole substrate (turnover) when the transporters are in a steady state phase with constant transporter-substrate complex concentrations. It is assumed that substrate binding and release are in

an equilibrium due to the fact that they take place in a much shorter time frame than the conformational changes of EcNhaA (rapid equilibrium approximation). So we can use the dissociation constants of Na^+ and H^+, K_D^{Na} and pK_a in an expression for binding equilibria (Fig. 6). In addition, the substrate transport is reversible and can therefore be described by the forward and backward rate constants k_1^+ and k_1^- for Na^+ and k_2^+ and k_2^- for H^+, which represent the conformational changes that determine the transport rate (Fig. 6).

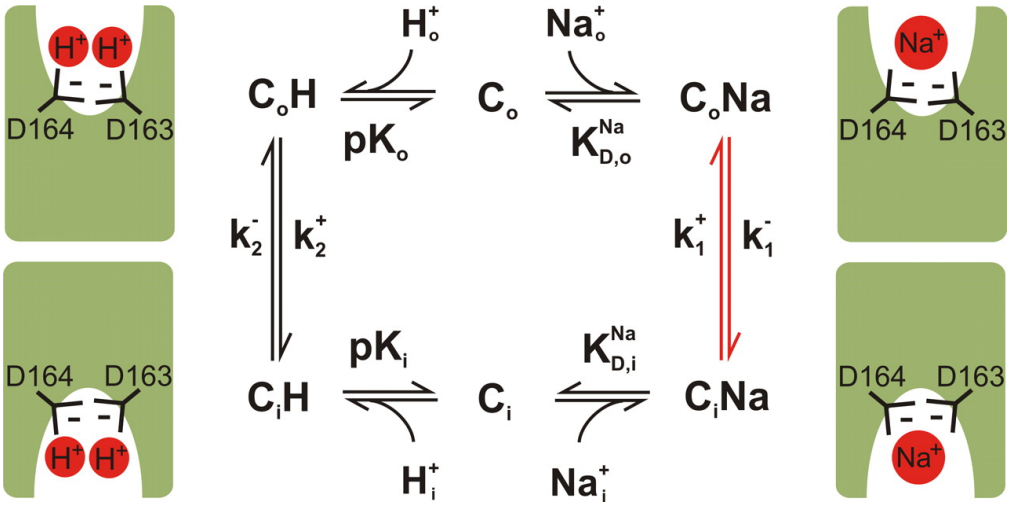

Figure 6: The minimal kinetic model of the EcNhaA transport mechanism including a single common binding site for Na^+ and H^+. C_o and C_i represent the outside and inside facing conformations. H^+ transport on the left, Na^+ on the right with a net charge transport indicated by red arrows. Image taken from Mager et al., 2011.

In this thesis the E241C EcNhaA were facing RSO (right-side out oriented proteoliposomes according to Zuber et al., 2005) and the transport in reverse mode was recorded.

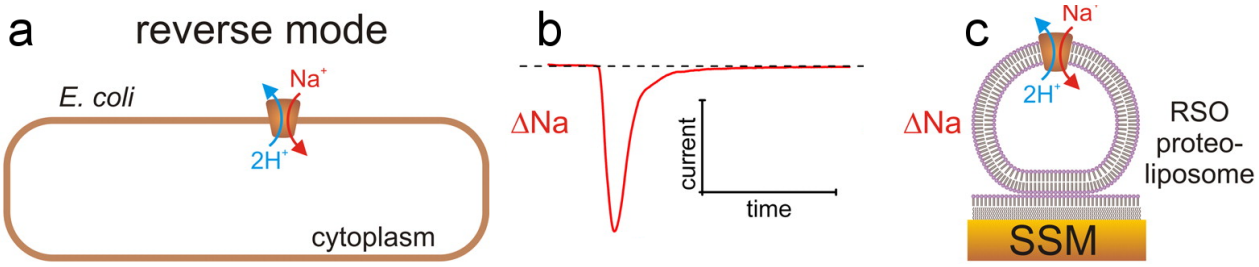

Figure 7: Graphical representation of EcNhaA in reverse transport mode in vivo (a) and reconstituted into proteoliposome (c). (b) Exemplary negative transient current of ΔNa^+ driven transport. Image modified after Mager et al., 2011.

4 Experimental Results

4.1 Functional characterisation of E241C EcNhaA

The functional characterization of E241C EcNhaA using RSO proteoliposomes was investigated by means of Na^+ concentration gradient driven transport in the reverse mode at symmetrical pH values between pH 6 and pH 9.5. The size of the Na^+ solution exchange artifacts was linearly dependent on Na^+ concentrations. Measurements were carried out at room temperature.

4.1.1 pH Dependence

The transient currents were measured after 10 mM and 100 mM Na^+ concentration jumps. Due to transport stochiometry currents are negative (Fig. 7). After a 100 mM Na^+ concentration jump at pH 8.5 peak currents of -3 nA ± 0.5 nA and at pH 7 peak currents of -0.3 nA ± 0.15 nA were recorded (Fig. 8, left image). The currents displayed monophasic behaviour. Only below pH 7 slight biphasic currents were measurable due to positive Na^+ solution exchange artifacts (see 3.4.2). The E241C EcNhaA activity displayed a bell-shaped pH dependence (Fig. 8, right image). E241C EcNhaA has its pH optimum at pH 8.8. The transporter current behaviour was reversible over the whole measured pH range.

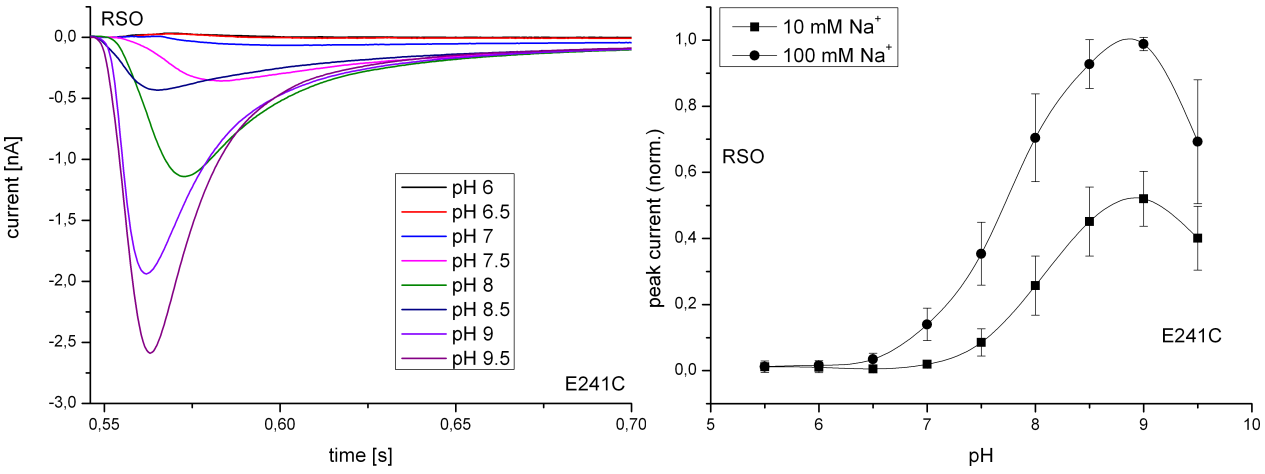

Figure 8: pH dependent transport activity of E241C EcNhaA in reverse mode using RSO proteoliposomes (LPR = 10). Left image: Exemplary transient currents after 100 mM Na^+ concentration jump. Na^+ transport produced negative currents according to transport stochiometry (Table 1 and Fig. 7). Right image: pH dependence at 10 mM and 100 mM Na^+ concentrations. Peak currents of three measurement series were artifact-corrected, averaged and normalized (see 3.4.2 and 3.5.1). Both images created with *Origin 8.5, Origin Labs.*

4.1.2 Na^+ Dependence

Transport activity of E241C EcNhaA decreases at acidic pH. To reveal information about the mechanism of activity decline, Na^+ dependencies of Na^+ gradient driven transport at pH 9 and pH 7.5 were measured. A hyperbolic fit (Fig. 9) allowed the identification of the K_m^{Na} for a constant Na^+ concentration saturation value of 1, because the I_{max} varied significantly between the measurement series due to different proteoliposome adsorptions. An increase of a $K_m^{Na} = 4.5 \pm 1.1$ mM at pH 9 to a $K_m^{Na} = 25.5 \pm 3.5$ mM at pH 7.5 could be detected. A comparison of the I_{max} values during measurement series on single sensors (see 3.5.2) revealed a change of v_{max} by 3%.

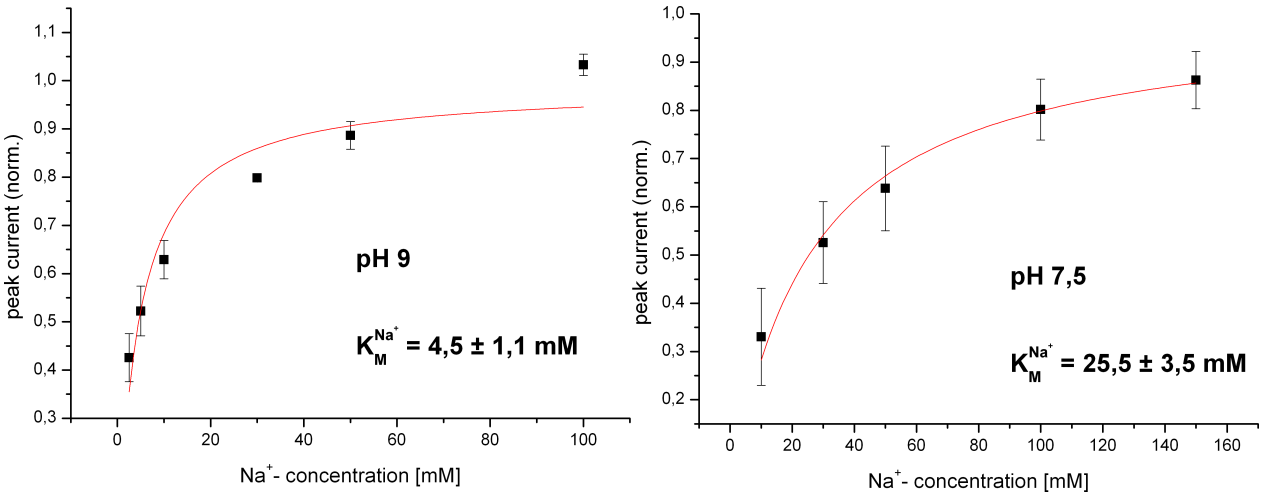

Figure 9: Na^+ concentration dependence of E241C EcNhaA at pH 9 (left image) and at pH 7.5 (right image) using RSO proteoliposomes. The transient currents were recorded after Na^+ concentration jumps. Peak currents of three independent measurement series were artifact-corrected, averaged and normalized. Hyperbolic fit with I_{max}=1. Images created with *Origin 8.5, Origin Labs.*

4.2 EcNhaA Inhibition with DEPC

6 mM diethylpyrocarbonate (DEPC) were added to each pH 7.5 and pH 9 buffer solutions and SSM measurements with 100 mM Na^+ were conducted. At pH 7.5 the peak currents at incubation time zero were at 0.5 nA. Shortly after the addition of DEPC the peak currents dropped down to a few pA within less than 50s (Fig. 10, left image). At pH 9 the peak currents at incubation time zero were at 2.4 nA. After addition of DEPC the peak currents decreased much more slowly to 80% of the initial amplitude after approximately 300s. The signal decreased with a progressively smaller rate and reached 0.5 nA after 100 minutes (Fig. 10, right image).

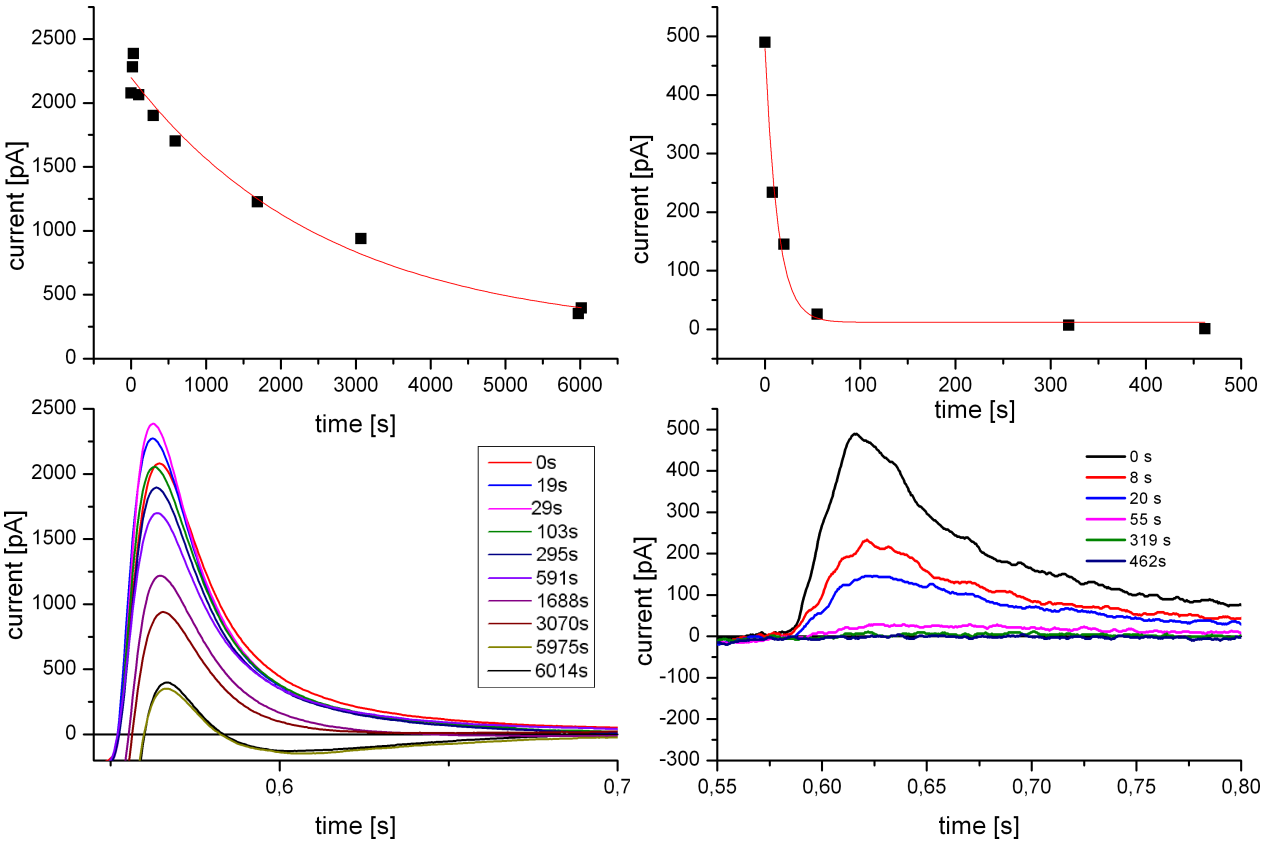

Figure 10: DEPC inhibition of E241C EcNhaA at pH 9 (left) and at pH 7.5 (right) using RSO proteoliposomes. Images created with *Origin 8.5, Origin Labs*.

5 Discussion

5.1 Transport Properties

5.1.1 Comparison of E241C with Wildtype EcNhaA

The optima of E241C and wildtype EcNhaA differ by 0.1 pH units on the basis of a Voigt peak fit of the pH dependencies of 100 mM Na^+ concentration gradient driven transport. The decrease of K_m^{Na} from pH 7.5 to pH 9 is approximately two times weaker for E241C EcNhaA as compared to the wildtype. The K_m^{Na} at pH 7.5 differs by a factor of four between E241C and wildtype EcNhaA. However, the bell-shaped pH dependence of the E241C mutant remains similar to the wildtype (Fig. 11). Therefore, and due to the insignificant shift of the pH optimum, no shift of the overall pH dependence for the E241C mutation at loop VIII-IX could be observed, which contradicts the allosteric model of EcNhaA pH response proposed by Gerchman et al. (1.4.3). Conversely, an explanation of the activity profile with the model of a competitive binding to a common binding site is valid for the E241C EcNhaA variant (cf. 1.4.3).

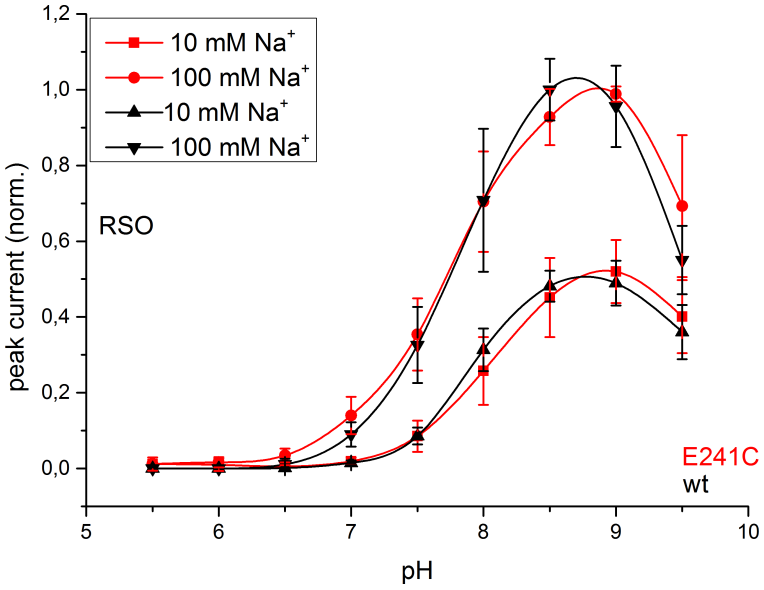

Figure 11: Comparison of the pH dependencies of E241C and wildtype EcNhaA at 10 mM and 100 mM Na^+ concentrations. Peak currents of three independent measurement series were artifact-corrected, averaged and normalized. Transport activity in reverse transport mode of E241C and wildtype EcNhaA in RSO proteoliposomes (LPR = 10).Wildtype data according to Mager et al. (2011).

Table 2: Comparison of transport parameters of wt and E241C EcNhaA. K_m^{Na} values were determined with hyperbolic fits of Na^+ dependencies at symmetric pH. Wildtype data from Mager et al., 2011.

EcNhaA	pH	K_m^{Na}	pH_{opt}
E241C	7.5	25.5 ± 3.5 mM	8.8
	9	4.5 ± 1.1 mM	
wt	7.5	102.2 ± 6.5 mM	8.7
	9	7.3 ± 1.1 mM	

5.1.2 Comparison with Fluorescence Dequenching Results

EcNhaA Activity Measurements with the Fluorescence Dequenching Method according to Gerchman et al., 1999. Acridine orange, a pH-sensitive fluorescent dye, is added to a solution containing native *E. coli* membrane vesicles with inside out orientation. When D-lactate is added and is subsequently dehydrogenated by the NAD-independent D-lactate-dehydrogenase (D-iLDH), the pH inside the vesicle decreases. Now the acridine orange that freely diffused across the vesicle membrane in its unprotonated form gets protonated and accumulates within the vesicle, as it cannot pass the membrane in its protonated form. In the course of the accumulation the fluorescence goes off due to quenching between the acridine orange molecules (Palmgren, 1991). If now Na^+ are added to the solution, they are transported by EcNhaA to the vesicle interior in exchange for 2 H^+ and the vesicle pH rises again, which leads to a deprotonation of acridine orange and its efflux and, by extension, a dequenching. The fluorescence signal rises again and is taken as a representation of the EcNhaA transport activity.

Potential Systematic Error of the Fluorescence Dequenching Measurements
The activity of D-iLDH is pH dependent, with a pH optimum for D-lactate oxidation in intact membrane vesicles of pH 6.2 to pH 6.8 (Kohn and Kaback, 1973; Futai, 1973). The different optima of D-iLDH and EcNhaA lead to a feedback wich creates different activity profiles of EcNhaA at different pH conditions. In addition it has been shown that the expression rates of different EcNhaA mutants vary (Gerchman et al., 1999).

5.2 Transport Inhibition with DEPC

The reason for conducting DEPC inhibition measurements with RSO E241C EcNhaA was to investigate signal inhibition during SSM electrophysilogical measurements. Earlier DEPC inhibition studies of EcNhaA using RSO vesicles demonstrated an inactivation of Na^+ transport (Damiano et al., 1985). DEPC is known to bind covalently to histidine, lysine, cysteine and tyrosine and to be susceptible to hydrolysis to ethanol and carbon dioxide in aqueous solutions, especially in the presence of nucleophiles such as in Tris or HEPES buffers (Berger et al., 1975). It has been shown that most of the DEPC modified amino acids have solvent-accessible surface area (SASA) percentages above 30% and modification rates of Tyr, Ser, Thr, Lys, and Cys were below 8% while their SASAs were above 50% (Mendoza et al., 2008) and are thus neglected here.

Table 3: Calculated solvent-accessible surface area (SASA) of possible DEPC modified EcNhaA residues based on EcNhaA crystal structure at pH 4 (PDB entry 1zcd, Hunte et al., 2005). His 253 and His 256 on TMS IX are potential solvent exposed residues. His 39 is potentially buried. Radius of water probe 1.4 Å. Calculated with *GETAREA* (Fraczkiewicz, R. and Braun, W., 1998)

amino acid residue	SASA [%]
His 39	7.8
His 225	21.6
His 243	21.5
His 253	86.0
His 256	52.4
His 318	29.4

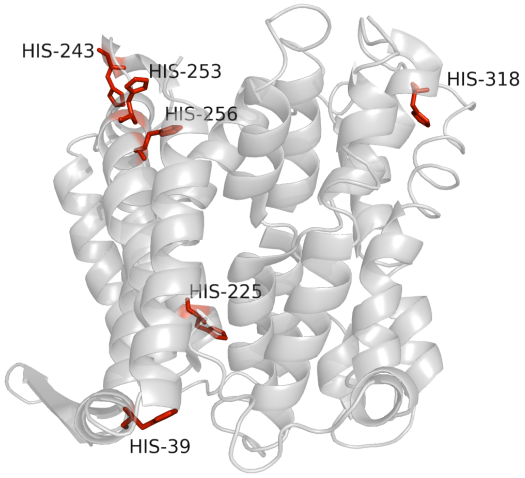

Figure 12: Cartoon model of EcNhaA at pH 4 with stick representation of histidine residues (red) representing the potential DEPC binding sites. Image created with *PyMOL, Schrödinger, Inc.*, based on PDB entry 1zcd (Hunte et al., 2005).

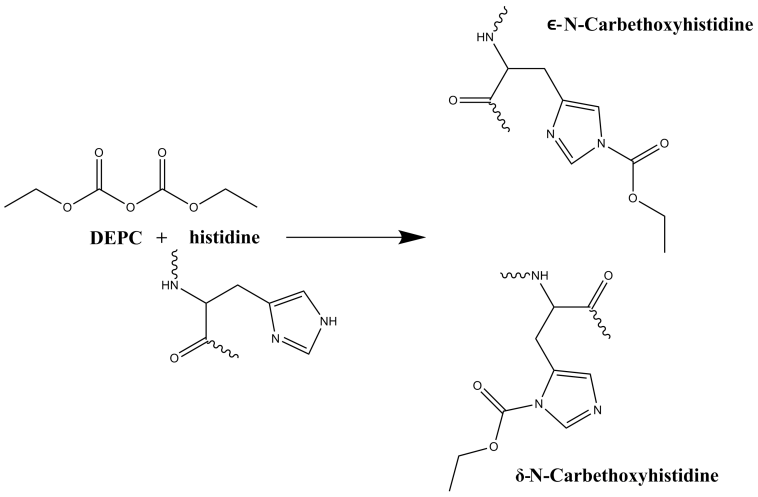

Figure 13: Formation of carbethoxyhistidine. DEPC attacks both δ-N and ϵ-N atoms of histidine (Narumi et al., 2012). Image created with *ChemBioDraw, Imagesoft.*

At pH 7.5 DEPC inhibition was most efficient, the signal ceased within less than 50 seconds (Fig. 10, right image). At pH 9 though, the inactivation occured partially with a much slower rate, the signal decreased by 50% only after 30 minutes (Fig. 10, left image). This might be due to the fact that DEPC reacts with histidine primarily between pH 6 and pH 8 (Mendoza et al., 2008). Together with the aforementioned hydrolysis of DEPC this might explain the remaining 10% of the initial signal after one hour.

5.3 Consensus with the Minimal Kinetic Model

It has been shown that a symmetrical minimal kinetic model presents a reasonable characterization of the H^+ and Na^+ dependencies of wildtype EcNhaA (Mager et al., 2011). The proportion of the rate constants ($\frac{k_2}{k_1} = 7$) represents a difference in the rate at which conformational changes elapse. From the increase of the K_m^{Na} at acidic pH (5.1.1 and Table 2) it can be deduced that a transport of Na^+ in the reverse direction at acidic pH is inhibited by competitive binding of H^+ to the binding site, preventing formation of C_oNa and, as a consequence, lowering the overall transport rate. On the other hand, at alkaline pH, the deficit of H^+ shifts the H^+ binding equilibrium at the cytoplasmic side of the transporter to the C_i form and as a result lowers the overall transport rate, too. A fit of the pH dependencies of E241C EcNhaA at 10 and 100 mM Na^+ concentrations to the minimal symmetrical kinetic model shows on the one hand that it describes well the pH dependence of E241C EcNhaA (Fig. 14) and on the other hand that the therewith calculated pK_a are virtually identical, with $pK_a = 8.7 \pm 0.1$ for E241C EcNhaA and $pK_a = 8.8 \pm 0.2$ for wildtype EcNhaA (Fig. 15). The K_D^{Na} differ by 2.9 mM, i.e. $K_D^{Na} = 5.5 \pm 2.0$ mM for E241C EcNhaA and $K_D^{Na} = 2.6 \pm 1.4$ mM for wt EcNhaA, which is within the error tolerance and thus insignificant. Consequently, the minimal symmetrical kinetic model produces similar dissociation constants for E241C EcNhaA and wildtype EcNhaA.

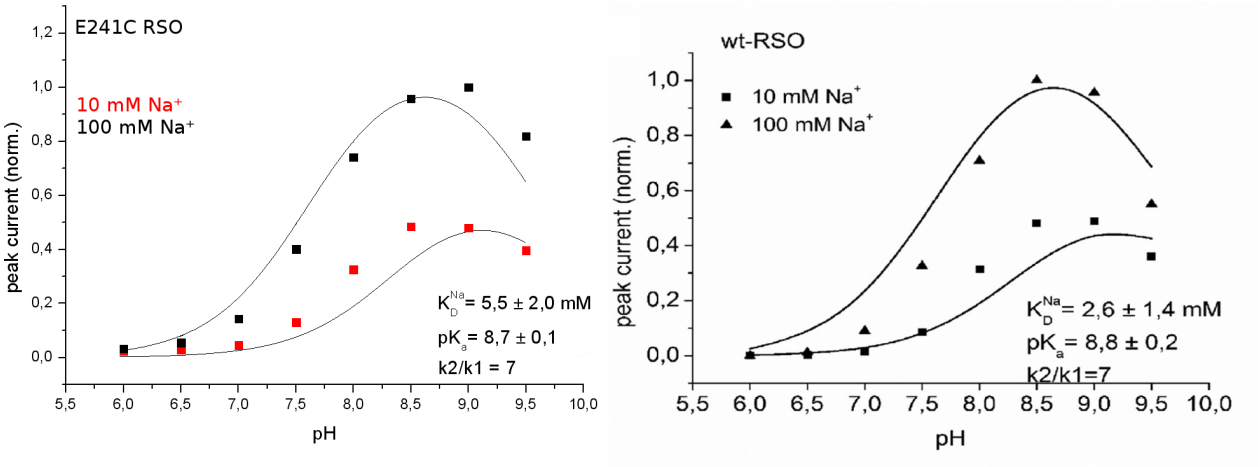

Figure 14: Fit of E241C EcNhaA (left image) and wildtype EcNhaA (right image, taken from Mager et al., 2011) pH dependencies at 10 and 100 mM Na^+ concentrations to the minimal kinetic model using RSO proteoliposomes. Calculations and graph done with *Origin 8.5, Origin Labs.*

6 Conclusion

pH and Na^+ dependence measurements of E241C EcNhaA displayed kinetic properties similar to wildtype EcNhaA (see 5.1.1). The K_m^{Na} showed an overall similar dependence on pH (see Table 2), v_{max} did not change significantly during measurement series (see 4.1.2), the optima are virtually identical (5.1.1) and an analytical solution of the kinetic equations based on the minimal symmetrical kinetic model (see 3.5.3) produced similar dissociation constants for E241C EcNhaA and wildtype EcNhaA (see 5.3, Figs. 14 and 15). Furthermore, the minimal symmetrical kinetic model validates the proposed model of a competitive binding of Na^+ and H^+ to a single binding site as it satisfactorily describes (see Fig. 14) the experimental data of E241C EcNhaA pH dependence gained in the course of this thesis. In light of the discrepancy between these results and the acidic shift observed by Gerchman et al. (see 1.5), a critical evaluation of the fluorescence dequenching method (see 5.1.2) revealed a potential systematic error in the fluorescence dequenching measurements. Different pH dependences of D-iLDH and EcNhaA and different expression rates of EcNhaA mutants may produce incoherent results (see 5.1.2). This suggests that pH conditions were not sufficiently defined in the fluorescence dequenching experiments. To conclude, the SSM electrophysiological study of E241C EcNhaA disproves an involvement of loop VIII-IX in pH regulation of EcNhaA activity and supports the proposed model of a single common binding site for Na^+ and H^+ responsible for both transport and pH regulation.

Appendix

References

1. Appel, M., D. Hizlan, K.R. Vinothkumar, C. Ziegler, and W. Kühlbrandt. 2009. Conformations of NhaA, the Na/H Exchanger from *Escherichia coli*, in the pH-Activated and Ion-Translocating States. Journal of Molecular Biology. 386: 351–365.

2. Berger, S.L. 1975. Diethyl pyrocarbonate: an examination of its properties in buffered solutions with a new assay technique. Analytical biochemistry. 67: 428–437.

3. Booth, I.R., W.J. Mitchell, and W.A. Hamilton. 1979. Quantitative analysis of proton-linked transport systems. The lactose permease of Escherichia coli. Biochemical Journal. 182: 687.

4. Brett, C.L., M. Donowitz, and R. Rao. 2005. Evolutionary origins of eukaryotic sodium/proton exchangers. American Journal of Physiology-Cell Physiology. 288: C223–C239.

5. Damiano, E., M. Bassilana, and G. Leblanc. 1985. Chemical modifications of the Na+ H+ antiport in Escherichia coli membrane vesicles. European Journal of Biochemistry. 148: 183–188.

6. Dover, N., C.F. Higgins, O. Carmel, A. Rimon, E. Pinner, et al. 1996. Na+ induced transcription of nhaA, which encodes an Na+/H+ antiporter in Escherichia coli, is positively regulated by nhaR and affected by hns. Journal of bacteriology. 178: 6508–6517.

7. Fendler, K., S. Jaruschewski, A. Hobbs, W. Albers, and J.P. Froehlich. 1993. Pre-steady-state charge translocation in NaK-ATPase from eel electric organ. The Journal of general physiology. 102: 631–666.

8. Fraczkiewicz, R., and W. Braun. 1998. Exact and efficient analytical calculation of the accessible surface areas and their gradients for macromolecules. Journal of Computational Chemistry. 19: 319–333.

9. Futai, M. 1973. Membrane D-lactate dehydrogenase from Escherichia coli. Purification and properties. Biochemistry. 12: 2468–2474.

10. Ganea, C., and K. Fendler. 2009. Bacterial transporters: Charge translocation and mechanism. Biochimica et Biophysica Acta (BBA) - Bioenergetics. 1787: 706–713.

11. Garcia-Celma, J.J., L. Hatahet, W. Kunz, and K. Fendler. 2007. Specific anion and cation binding to lipid membranes investigated on a solid supported membrane. Langmuir. 23: 10074–10080.

12. Gerchman, Y., A. Rimon, and E. Padan. 1999. A pH-dependent conformational change of NhaA Na+/H+ antiporter of Escherichia coli involves loop VIII–IX, plays a role in the pH response of the protein, and is maintained by the pure protein in dodecyl maltoside. Journal of Biological Chemistry. 274: 24617–24624.

13. Goldup, A., S. Ohki, and J.F. Danielli. 1970. Black lipid films. Progress in Surface and Membrane Science, Academic Press, New York. 3: 193–260.

14. Henzler-Wildman, K., and D. Kern. 2007. Dynamic personalities of proteins. Nature. 450: 964–972.

15. Hilger, D., H. Jung, E. Padan, C. Wegener, K.-P. Vogel, et al. 2005. Assessing Oligomerization of Membrane Proteins by Four-Pulse DEER: pH-Dependent Dimerization of NhaA Na+/H+ Antiporter of *E. coli*. Biophysical journal. 89: 1328–1338.

16. Hilger, D., Y. Polyhach, E. Padan, H. Jung, and G. Jeschke. 2007. High-Resolution Structure of a Na+/H+ Antiporter Dimer Obtained by Pulsed Electron Paramagnetic Resonance Distance Measurements. Biophysical journal. 93: 3675–3683.

17. Hunte, C., E. Screpanti, M. Venturi, A. Rimon, E. Padan, et al. 2005. Structure of a Na+/H+ antiporter and insights into mechanism of action and regulation by pH. Nature. 435: 1197–1202.

18. Kang, H.J., C. Lee, and D. Drew. 2013. Breaking the barriers in membrane protein crystallography. The international journal of biochemistry and cell biology. 45(3): 636-644.

19. Kohn, L.D., and H.R. Kaback. 1973. Mechanisms of Active Transport in Isolated Bacterial Membrane Vesicles XV. Purification and Properties of the Membrane-Bound D-Lactate Dehydrogenase from *Escherichia coli*. Journal of Biological Chemistry. 248: 7012–7017.

20. Krishnamurthy, H., C.L. Piscitelli, and E. Gouaux. 2009. Unlocking the molecular secrets of sodium-coupled transporters. Nature. 459: 347–355.

21. Mager, T., A. Rimon, E. Padan, and K. Fendler. 2011. Transport Mechanism and pH Regulation of the Na+/H+ Antiporter NhaA from *Escherichia coli*: An Electrophysiological Study. Journal of Biological Chemistry. 286: 23570–23581.

22. Mendoza, V.L., and R.W. Vachet. 2008. Protein surface mapping using diethylpyrocarbonate with mass spectrometric detection. Analytical chemistry. 80: 2895–2904.

23. Narumi, R., T. Yamamoto, A. Inoue, and T. Arata. 2012. Substrate-induced conformational changes in sarcoplasmic reticulum Ca2+ -ATPase probed by surface modification using diethylpyrocarbonate with mass spectrometry. FEBS letters. 586(19):3172-8.

24. Padan, E., T. Tzubery, K. Herz, L. Kozachkov, A. Rimon, et al. 2004. NhaA of *Escherichia coli*, as a model of a pH-regulated Na+/H+antiporter. Biochimica et Biophysica Acta (BBA) - Bioenergetics. 1658: 2–13.

25. Padan, E., L. Kozachkov, K. Herz, and A. Rimon. 2009. NhaA crystal structure: functional-structural insights. Journal of Experimental Biology. 212: 1593–1603.

26. Palmgren, M.G. 1991. Acridine orange as a probe for measuring pH gradients across membranes: mechanism and limitations. Analytical biochemistry. 192: 316–321.

27. Pinner, E., E. Padan, and S. Schuldiner. 1994. Kinetic properties of NhaB, a Na+/H+ antiporter from Escherichia coli. Journal of Biological Chemistry. 269: 26274–26279.

28. Rath, A., M. Glibowicka, V.G. Nadeau, G. Chen, and C.M. Deber. 2009. Detergent binding explains anomalous SDS-PAGE migration of membrane proteins. Proc. Natl. Acad. Sci. U.S.A. 106: 1760–1765.

29. Schulz, P., J.J. Garcia-Celma, and K. Fendler. 2008. SSM-based electrophysiology. Methods. 46: 97–103.

30. Screpanti, E., E. Padan, A. Rimon, H. Michel, and C. Hunte. 2006. Crucial Steps in the Structure Determination of the Na+/H+ Antiporter NhaA in its Native Conformation. Journal of Molecular Biology. 362: 192–202.

31. Singer, S.J., and G.L. Nicolson. 1972. The fluid mosaic model of the structure of cell membranes. Science. 175: 720–731.

32. Taglicht, D., E. Padan, and S. Schuldiner. 1991. Overproduction and purification of a functional Na+/H+ antiporter coded by nhaA (ant) from Escherichia coli. Journal of Biological chemistry. 266: 11289–11294.

33. Taglicht, D., E. Padan, and S. Schuldiner. 1993. Proton-sodium stoichiometry of NhaA, an electrogenic antiporter from *Escherichia coli*. Journal of Biological Chemistry. 268: 5382–5387.

34. West, I.C., and P. Mitchell. 1974. Proton/sodium ion antiport in *Escherichia coli*. Biochemical Journal. 144: 87.

35. Zhao, Y., D.S. Terry, L. Shi, M. Quick, H. Weinstein, et al. 2011. Substrate-modulated gating dynamics in a Na+ coupled neurotransmitter transporter homologue. Nature. 474: 109–113.

36. Zuber, D., R. Krause, M. Venturi, E. Padan, E. Bamberg, et al. 2005. Kinetics of charge translocation in the passive downhill uptake mode of the Na+/H+ antiporter NhaA of *Escherichia coli*. Biochimica et Biophysica Acta (BBA)-Bioenergetics. 1709: 240–250.

Acknowledgements

Thanks to Prof. Dr. Klaus Fendler for giving me the opportunity to perform the experiments in his laboratory under the supervision of his research group. I really appreciate the confidence and patience that has been granted to me.

Thanks to Dr. Thomas Mager and Lina Hatahet for the magnificent support and sharing of knowledge in the course of the experiments.